






Article

Macrophage in vitro Response on Hybrid Coatings Obtained by Matrix Assisted Pulsed Laser Evaporation

Madalina Icriverzi ^{1,2} , Laurentiu Rusen ³ , Simona Brajnicov ^{3,4}, Anca Bonciu ^{3,5} , Maria Dinescu ³, Anisoara Cimpean ² , Robert W. Evans ⁶, Valentina Dinca ^{3,*}  and Anca Roseanu ^{1,*}

¹ Institute of Biochemistry, Romanian Academy, 296 Splaiul Independentei, 060031 Bucharest, Romania; radu_mada@yahoo.co.uk

² Faculty of Biology, University of Bucharest, Splaiul Independentei 91-95, 050095 Bucharest, Romania; anisoara.cimpean@bio.unibuc.ro

³ National Institute for Lasers, Plasma and Radiation Physics, Atomistilor 409, 077125 Magurele, Bucharest, Romania; laurentiu.rusen@inflpr.ro (L.R.); brajnicov.simona@inflpr.ro (S.B.); anca.bonciu@inflpr.ro (A.B.); maria.dinescu@inflpr.ro (M.D.)

⁴ Faculty of Mathematics and Natural Sciences, University of Craiova, 200585 Craiova, Romania

⁵ Faculty of Physics, University of Bucharest, RO-077125 Magurele, Bucharest, Romania

⁶ School of Engineering and Design, Brunel University, London UB8 3PH, UK; robertwevans49@gmail.com

* Corresponding: valentina.dinca@inflpr.ro (V.D.); roseanua@gmail.com (A.R.)

Received: 28 February 2019; Accepted: 2 April 2019; Published: 4 April 2019



Abstract: The improvement in the research area of the implant by surface functionalization when correlated with the biological response is of major interest in the biomedical field. Based on the fact that the inflammatory response is directly involved in the ultimate response of the implant within the body, it is essential to study the macrophage-material interactions. Within this context, we have investigated the composite material-macrophage cell interactions and the inflammatory response to these composites with amorphous hydroxyapatite (HA), Lactoferrin (Lf), and polyethylene glycol-polycaprolactone (PEG-PCL) copolymer. All materials are obtained by Matrix Assisted Pulsed Laser Evaporation (MAPLE) technique and characterized by Atomic Force Microscopy and Scanning Electron Microscopy. Macrophage-differentiated THP-1 cells proliferation and metabolic activity were assessed by qualitative and quantitative methods. The secretion of tumor necrosis factor alpha (TNF- α) and interleukin 10 (IL-10) cytokine, in the presence and absence of the inflammatory stimuli (bacterial endotoxin; lipopolysaccharide (LPS)), was measured using an ELISA assay. Our results revealed that the cellular response depended on the physical-chemical characteristics of the coatings. Copolymer-HA-Lf coatings led to low level of pro-inflammatory TNF- α , the increased level of anti-inflammatory IL-10, and the polarization of THP-1 cells towards an M2 pro-reparative phenotype in the presence of LPS. These findings could have important potential for the development of composite coatings in implant applications.

Keywords: composite coatings; MAPLE; Lactoferrin; macrophage interactions

1. Introduction

The success of a bone implant material is dependent on the host immune response. Following injury or implantation of a biomaterial, there is an infiltration of inflammatory cells at the site of the wound. Monocyte-derived macrophages [1] are among the first cells that interact and react to implanted biomaterials, playing a role in the inflammatory response and orchestration of tissue repair [2–6].

They are key cells involved in the control and modulation of the inflammatory response associated with the host tissue response to foreign bodies [7–9]. The cellular response may range from the immune stimulator to the immune suppressor depending on the polarization state of macrophages determined by environmental factors and parameters of the biomaterials [10]. Geometry, topography, hydrophobicity or surface chemistry, as well as the mechanical properties or composition of the materials, are characteristics that influence the response of macrophages [6,11–15].

The macrophage phenotype is roughly divided into two distinct populations: M1 pro-inflammatory, classically activated macrophages and M2 anti-inflammatory, alternatively-activated macrophages. The classification is done according to *in vitro* stimulation, released cytokines, receptors expressed on the cell surface, as well as enzyme activity [2,16–21]. Thus, the M1 type can be activated *in vitro* by the stimulation of lipopolysaccharide (LPS), and secretes pro-inflammatory cytokines like tumor necrosis factor alpha (TNF- α) and exhibits predominantly C-C chemokine receptor type 7, CCR7 cellular marker. The M2 phenotype associated with wound healing and tissue repair is activated *in vitro* by IL-4 or IL-13 cytokines, and secretes mainly IL-10 and expresses mannose receptor CD206, Cluster of Differentiation 206 [16,19,21–23].

To optimize the response of bone biomaterials and avoid excessive inflammation or implant rejection, different immunomodulation approaches have been adopted to interfere with the immune system [24–30].

An innovative strategy to increase the efficacy of a biomaterial with medical applications could be its coating with a natural protein or a biological compound. Unlike the case of injection of a bioactive compound that is usually rapidly removed from the body, depositing the protein on the surface of the implanted material causes an increase in its concentration and results in a controlled local release. This approach may also help to prevent post-surgical infection in bone implants [31] and favor a local induction of osteogenic differentiation.

Different types of biomaterials with specific characteristics are used as drug carriers for efficient delivery of a biomolecule to a specific target [32]. It is worth mentioning that new strategies have emerged to implement therapies with enhanced drug accumulation in the targeted tissue area and decreased side effects [33,34]. Biomaterials, designed for hard tissue engineering and regeneration, exploit different strategies for spatially and temporarily controlled drug delivery with osteoimmunomodulatory properties for efficient osteogenic regeneration [35].

One protein of practical interest is lactoferrin (Lf), which, besides its antimicrobial and anti-carcinogenic activities, also has an anti-inflammatory function and an osteogenic role [36,37]. Lf released at the site of injury interacts with microbial elements and with cells of the immune system, affecting them at both the cellular and molecular level [38–44]. The protein also plays an important role in the activity of bone cells, as it shows anti-apoptotic and differentiation effects on osteoblasts and an inhibitory effect on osteoclastogenesis [45–47].

It was recently shown that implants coated with different hydroxyapatite (HA) forms, crystalline or amorphous, can trigger different inflammatory responses related to surface chemistry and morphology [48,49]. Moreover, HA in combination with other growth factors, proteins or polymers has been used for studying the influence on both inflammatory and osteogenic responses. Thus, different studies have been performed with Lf-HA functionalized nanocrystals [50,51] revealing this combination as a promising system with anti-inflammatory properties and increased osteogenic capacity. It has been proved that biomimetic HA nanocrystals surface-functionalized with Lf have antibacterial activity effective against Gram-positive and Gram-negative bacteria [52–54].

There are various deposition methods which can be used for coating a surface, from click chemistry to physical simple methods, such as spin-coating, or more complex procedures, such as laser deposition [55–65]. The main disadvantages for most of the techniques are the poor control over thickness and roughness, lack of possibility to include proteins or growth factors within a wide range of synthetic polymeric matrices, or the fact that the methods imply toxic precursors, causing the

destruction of the bio-compounds. There are also limited options when composite materials containing organic polymers, ceramics, and proteins are required.

In recent years, Matrix Assisted Pulsed Laser Evaporation (MAPLE) has been used for depositing single component coatings constituted of simple polymers to functional *Micrococcus* bacteria for a wide range of applications. MAPLE technique is derived from Pulsed Laser Evaporation, except it is using a frozen target that consists of a solution of the material of interest dissolved or suspended in a solvent (final concentration maintained below 5% (*w/v*)). The choice of solvent is based on its volatility and ability to absorb the wavelengths used, without the denaturation of the material. During the deposition process, the laser beam is scanned on the target surface, the laser beam energy being absorbed by the frozen solvent, therefore vaporizing it and transferring the target molecules toward and onto the substrate placed parallel and at a distance of few cm from the target. Depending on the number of pulses and target composition, there is a deposition/growth of a thin film on the surface of the substrate, while the solvent molecules are pumped away [57–64]. Moreover, MAPLE was shown to be an appropriate approach for obtaining hybrid coatings by embedding, in a controlled way, ceramic material, graphene, nanoparticles within a natural or synthetic polymer layer [57–64].

We recently demonstrated the potential of the MAPLE technique for single-step deposition of multiple bioactive factors as an embedding process into a biodegradable synthetic polymeric thin film (PEG-PCL-Me, Co). The major advantage of the technique was the lack of influence of solvents or specific deposition conditions on the functionality of proteins or drugs [57,58]. It was demonstrated that by entrapping the osteoconductive factors, HA and Lf, within a biodegradable copolymer matrix of PEG-PCL-Me, high performances of the multifunctional biomimetic coatings, such as enhanced proliferation, differentiation, and survival of osteoblasts, were achieved [58].

As previously mentioned, the inflammatory response can dictate the final response of the implant within the body. Therefore, a good understanding of macrophage interactions with a specific substrate could bring important information on the tailoring of material surfaces that could have an impact on further applications within biomedical devices.

Within this context, our study aimed to investigate the material-macrophage cell interactions and the inflammatory response to composites containing amorphous HA, Lf, and the polyethylene glycol-polycaprolactone (PEG-PCL) copolymer.

2. Materials and Methods

2.1. Materials

Poly (ethylene glycol)-*block*-poly(ϵ -caprolactone) methyl ether (570303 Aldrich) (PEG-*block*-PCL Me -average $M_n \sim 5,000$, PCL average $M_n \sim 5,000$), Lf lyophilized powder (L0520 SIGMA), and HA powder (677418 Aldrich) were obtained from Sigma-Aldrich (Saint Louis, MO, USA).

2.2. Coatings Deposition and Surface Characterization

Composite coatings were obtained by the MAPLE technique and the triple module target system, as previously described [54]. Briefly, a “Surelite II” pulsed Nd:YAG laser system (Continuum Company, Pessac, France) (266 nm, 6 ns pulse duration, 10 Hz repetition rate) was used at a fluence of 450 mJ/cm² (for 0.02 cm² laser spot size measured on the target surface) to irradiate in a single step a modular target consisting of frozen solutions of PEG-*block*-PCL Me copolymer (Co), Lf, HA (Sigma-Aldrich, Saint Louis, MO, USA).

Taking into consideration that the reported Lf concentration in the blood circulation is normally below 1 μ g/mL, but significantly increased in inflammation/injury process, even up to 70 μ g/mL [66], an intermediate value of 10 μ g of Lf per sample was used. In order to ensure uniform coverage of the surfaces and sufficient polymeric layer to entrap the two bioactive components, the number of pulses/sample was chosen according to the material type: 45,000 pulses for Lf, 30,000 pulses for PEG-PCL-Me, and 30,000 pulses for HA, leading to the quantities of deposited materials of 10 μ g for Lf

protein and 67 µg for HA. Nevertheless, for HA, the ratio Ca/P calculated according to energy dispersive X-ray analysis (EDAX) for those conditions was close to that of bone, namely 1.58. PEG_PCL Me copolymer was used due to its ability to start degrading within the first 24 h due to PEG component, as well to maintain the coating for longer periods than 1 month when deposited as thin films [58]. Moreover, based on FTIR measurements, it was shown that the functional groups of all the elements were maintained both after MAPLE process and incorporation of LF and HA within PEG-PCL copolymer matrix, which gives an important advantage for the controlled release of functional bio-components [58].

For the single component coatings, each solution was well homogenized and rapidly frozen in a liquid nitrogen-cooled copper container. The modular target system for embedding HA and Lf in the copolymer coatings included one or two Teflon rings (concentric). Each material was frozen separately and removed after freezing, so no interaction occurred between Teflon and the laser beam during experiments [58]. Glass substrates were cleaned in acetone, ethyl alcohol, and finally deionized water and dried before being placed in the deposition chamber. The target obtained was then mounted on a copper holder inside the deposition chamber and maintained in a frozen state by liquid nitrogen. In order to avoid local damages due to overheating and drilling as a result of the laser irradiation, the target was rotated during the deposition time. The distance between the substrates and the target was kept at 3 cm. The vapors of the solvents were extracted from the chamber by a vacuum pump.

The nano- and micro-topographical characteristics were analyzed by Atomic Force Microscopy AFM (XE 100 AFM setup from Park System, Suwon, Korea) and Scanning electron microscopy (SEM) (JEOL Ltd, Tokyo, Japan). Surface and roughness measurements were performed in a non-contact mode. For each coating type, 5 areas were randomly selected and measured. SEM was performed using a JSM-531 microscope (5 kV). The contact angles were measured by the sessile drop method, and the reported values were obtained upon averaging 5 measurements performed on different areas of the sample, at 60 s time interval to obtain a steady-state value.

2.3. Cell Culture Model

Human THP-1 cells (ATCC, CRL-12424) were maintained in RPMI 1640 medium with 10% (*v/v*) inactivated fetal bovine serum (FBS) and 1% (*v/v*) streptomycin/penicillin at 37 °C in a humidified atmosphere of 5% CO₂. For in vitro biological assessment, THP-1 cells were cultured on material surfaces at a density of 4×10^5 cells/surface material in 24-well plates (NUNC). Macrophages were generated from monocytic THP-1 cells by incubation for 72 h with 100 ng/mL *phorbol* 12-myristate 13-acetate (PMA). Materials with adherent THP-1-derived macrophages were moved to a new 24-well plate and incubated for 4 h (resting phase) with glutamine-free RPMI medium supplemented with 5% (*v/v*) FBS. Cells were maintained with or without 50 ng/mL *lipopolysaccharide* LPS (*Escherichia coli* 055:B5, Sigma L4524) for a further 18 h to simulate pro-inflammatory and non-inflammatory experimental conditions.

2.4. Cell Viability and Proliferation

Before all biological experiments, the coatings were sterilized by immersion in 1% Penicillin-Streptomycin solution for 15 min.

The proliferation of THP-1 cells cultured on the material surface was evaluated by the MTS assay (CellTiter 96® AQueous One Solution Cell Proliferation Assay, Promega, Fitchburg, WI, USA), which is based on reduction of a tetrazolium compound (3-(4,5-dimethylthiazol-2-yl)-5-(3-carboxymethoxyphenyl)-2-(4-sulfophenyl)-2H-tetrazolium) to formazan by a dehydrogenase present in the metabolically active cells. The amount of formazan released into the culture medium is proportional to the number of live cells. Macrophage-differentiated THP-1 cells treated or not treated with LPS were incubated with MTS solution at 37 °C. After 15 min, 100 µL of supernatant was transferred to a 96-well plate, and the optical density was measured at 450 nm using a microplate reader (Mithras Berthold LB 940, Berthold Technologies, Bad Wildbad, Germany). The viability of THP-1 cells grown on biomimetic surfaces was investigated using the LIVE/DEAD viability/cytotoxicity kit (Molecular Probes, Eugene, OR, USA). Cells were incubated for 30 min with 10 µM Calcein AM (calcein AM) and

4 μ M Ethidium homodimer-1 (EthD-1) in complete RPMI medium. Subsequently, the samples were fixed with 4% paraformaldehyde (PFA) for 15 min. The nuclear labeling was carried out with Hoechst dilution 1:3000 (Life Technologies, Eugene, OR, USA) for 1 min. Negative controls (cell death) were obtained by the treatment of differentiated THP-1 cells with 70% ethanol for 5 min. The samples were mounted with ProLong Gold Antifade Reagent (Molecular Probes, Life Technologies, Eugene, OR, USA) and immediately visualized with the 10 \times objective using the Zeiss AxioCam ERc5s ApoTome microscope (Jena, Germany) with ApoTome.2 cursor mode. Representative images were captured with the AxioVision Rel 4.8 program that controls the camera AxioCam MRm (Jena, Germany).

2.5. Cell Adhesion and Morphology

The coating effect on macrophage morphology and spreading was investigated by fluorescence microscopy following the distribution of actin and vinculin filaments. Macrophages attached to the surfaces in the presence or absence of LPS were fixed for 15 min with 4% PFA, permeabilized with 0.2% Triton X-100, blocked for one hour with 0.5% BSA-PBS (bovine serum albumin-phosphate buffered saline), and then washed with PBS. Actin filaments were stained with Alexa Fluor 488 Phalloidin (green) (Invitrogen, Thermo Fisher Sci., CA, USA) for one hour at room temperature (RT) in 0.5% BSA-PBS solution. Vinculin labeling was performed for 30 min with a mouse anti-human antibody (Sigma) diluted at 1:50 in 0.5% BSA-PBS buffer and subsequently with Alexa Fluor 594-conjugated goat anti-mouse antibody (red) (Life Technologies) dilution 1:400 in the same buffer for 30 min. The nuclei were counterstained with Hoechst fluorescent dye (blue) (1:3000 in PBS) for 1 min at room temperature. After repeated washing with PBS, the samples were mounted on a microscope slide with ProLong Gold antifade (Molecular Probes, Life Technologies), an agent that allows the fluorescence signal to be maintained over a prolonged period. Samples were examined using 20 \times and 40 \times lens of Zeiss AxioCam ERc5s ApoTome microscope with ApoTome.2 cursor mode and AxioVision 4.8 software (Zeiss).

For scanning electron microscopy, THP-1 differentiated macrophage human cells cultured on the surface of composite materials were washed with PBS and fixed with 2.5% glutaraldehyde solution in PBS for 20 min. The samples were then subjected to gradient dehydration with 70%, 90%, and 100% ethanol solutions in two rounds of 15 min for each concentration followed by two rounds of 3 min incubation with 50%, 75% hexamethyldisilazane (HDMS, in ethanol), and then 100% HDMS solution. Evaporation of the HDMS solution was carried out in a Euroclone AURA 2000 M.C. An Inspect S Electron Scanning Microscope (FEI Company, Hillsboro, OR, USA) was used to obtain the electron microscopy images.

2.6. Cytokine Secretion Profile

The level of pro- and anti-inflammatory cytokines, TNF- α and IL-10, respectively, in cell supernatants (stored at -80°C) was determined by the sandwich enzyme-linked immunosorbent assay (ELISA) method after 18 h of incubation with or without LPS (*E. coli*) bacterial endotoxin. The commercially available ELISA assay kit for the TNF- α and IL-10 cytokines from the R&D System, (Minneapolis, MN, USA) was used following the manufacturer's specifications. Briefly, the experiments were performed in 96-well plates (MaxiSorp, Nunc, Thermo Fisher Sci., CA, USA) treated at room temperature for 24 h with anti-TNF- α and IL-10 specific monoclonal antibodies (R&D System). After repeated washing with 0.05% Tween-PBS and blocking with 1% BSA in PBS, cell supernatants were incubated for 2 h at room temperature followed by a 2 h incubation with detection antibodies hTNF- α and hIL-10 coupled with biotin. The streptavidin-HRP conjugate and the H_2O_2 : TMB enzyme substrates (BD Biosciences, Becton, Dickinson and Company, East Rutherford, NJ, USA) were used to measure the cytokine level in the cell environment. The enzyme reaction was stopped with H_2SO_4 2 N, and the optical density was measured at 450 nm (monitored by extinction reading at 450 nm) on the Mithras LB 940 DLReady spectrophotometer (BERTHOLD TECHNOLOGIES GmbH & Co. KG, Wildbad, Germany). To eliminate the variation of cell density and viability on each surface, the amount of released cytokines was normalized and expressed in relation to the results obtained in

the cell viability assay against the control material. The cytokine concentration was calculated using the formula: $\text{pg/mL normalized} = \text{pg/mL measured} \times (\text{DO MTS control}/\text{DO MTS sample})$.

2.7. Macrophage Polarization on Material Surfaces

The ability of macrophages to polarize on different coatings in the presence or absence of bacterial endotoxin was investigated by fluorescent labeling of specific markers. Thus, cells were fixed for 15 min with 4% PFA, blocked for one hour with 0.5% BSA-PBS (reagent diluent), and then washed with PBS. For chemokine type 7, macrophage M1 marker and for mannose receptor, macrophage M2 marker staining, the samples were incubated with human anti-CCR7 monoclonal antibodies and human anti CD206 antibodies (R&D systems), diluted 1:50 for 30 min at room temperature in reagent diluent. Subsequently, the samples were incubated for 30 min with anti-mouse antibodies coupled with Alexa-Fluor 594 and the anti-goat antibody coupled with Alexa-Fluor 488 (Life Technologies, 1:400 dilutions). The nuclear staining was made with the Hoechst (1: 3000 dilutions in PBS solution) for 1 min at RT, and samples were mounted on a microscope slide with ProLong Gold antifade (Molecular Probes, Life Technologies). Samples were inspected with a 40x objective (Zeiss AxioCam ERc5s ApoTome microscope with ApoTome.2 cursor mode), and the representative images were captured using AxioCam MRm camera controlled by AxioVision Rel 4.8 program.

2.8. Statistical Analysis

Data were collected from triplicate samples, and the results were expressed as mean values \pm SD. Significant differences with p -value < 0.05 between results were analyzed with GraphPad Prism software (version 5; La Jolla, CA, USA) using one-way ANOVA or two-way ANOVA with Bonferroni's multiple comparison tests.

3. Results and Discussion

3.1. Surface Characterization of Composite Coatings

The chemical characterization of deposited surface used in the present work was previously described [54]. However, the reduction of a number of pulses used led to a decrease of both Lf and HA within the sample which have determined changes in the coatings morphology (Figure 1). A more detailed view and changes related to the roughness of the samples are shown in Figure 2 for a single element and for composites coatings. It can be observed that the previously observed trends, based on the composition, are maintained, with some differences in the mediated roughness of the samples containing Lf and HA. The morphology of the coatings consisted, in full coverage, of the substrates, with some random island-like structures for the Lf and Co samples, while those based on HA had the accumulation of nanoparticles onto the surface. The overview of the top morphology is shown in Figure 1.

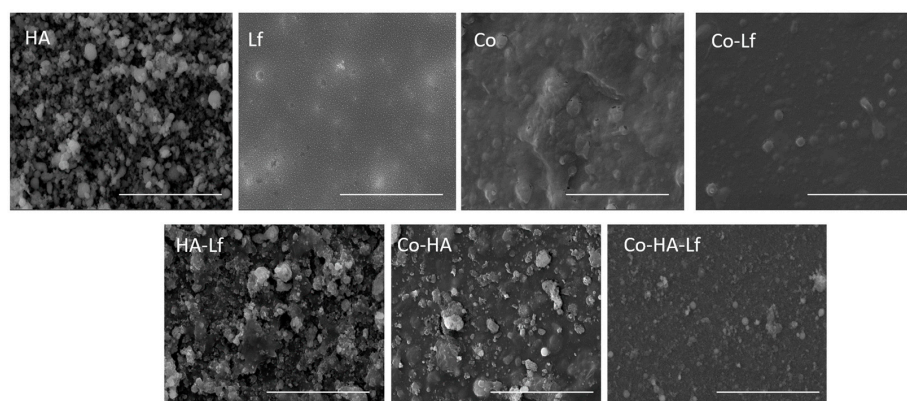


Figure 1. SEM images of the top morphology of the coatings obtained by Matrix Assisted Pulsed Laser Evaporation (MAPLE). Scale bar: 10 μm . HA: hydroxyapatite; Lf: lactoferrin.

In addition, the decrease of Lf and HA within the surface of the samples did lead to roughness and hydrophilicity changes unlike in the previously reported samples. In fact, the corresponding AFM images also showed distinct features for the composite, with the surface root mean square roughness results (obtained from the AFM measurements), revealing increased roughness, clearly indicating that surface morphology and microstructure can change depending on composition.

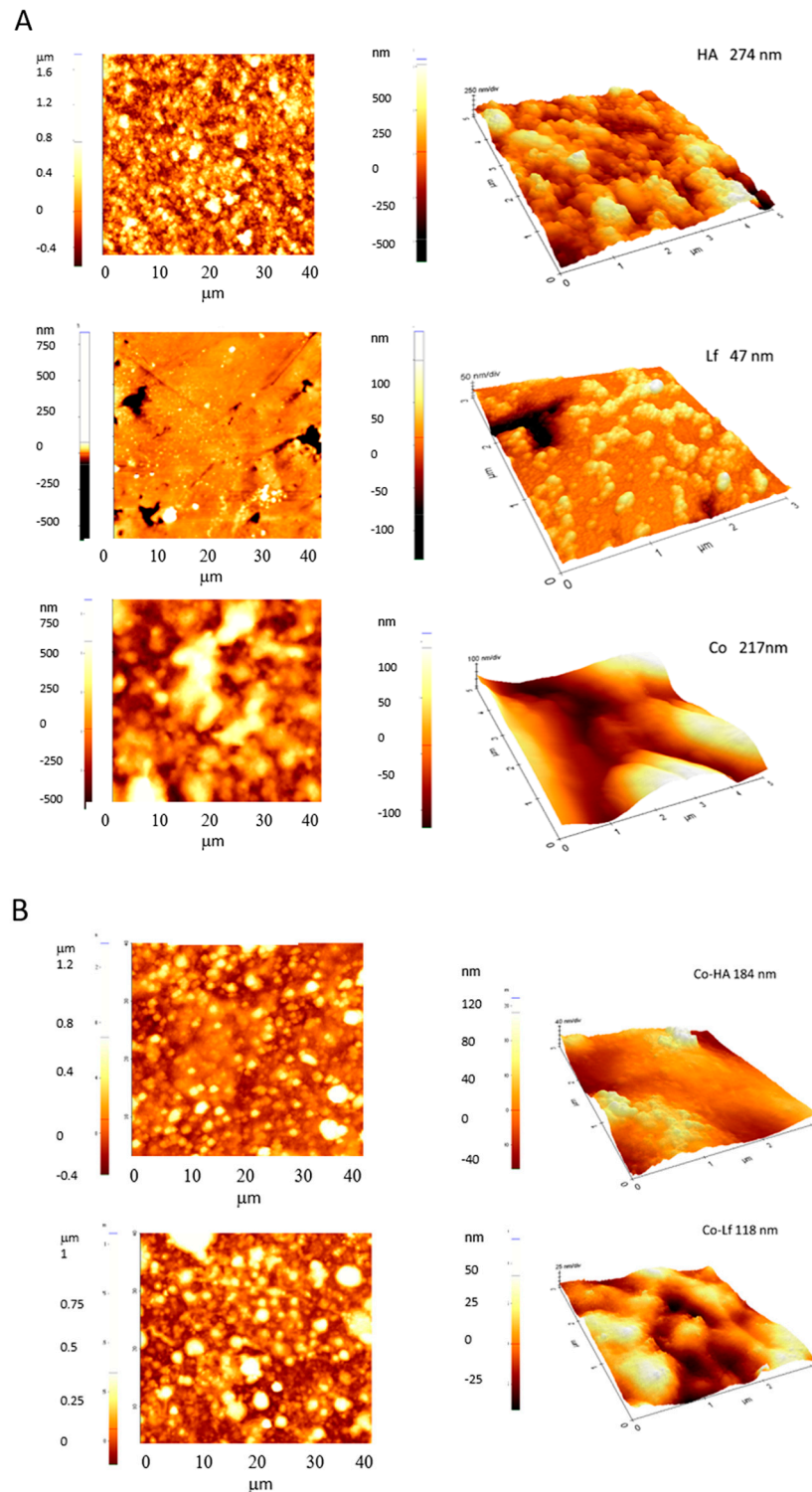


Figure 2. Cont.

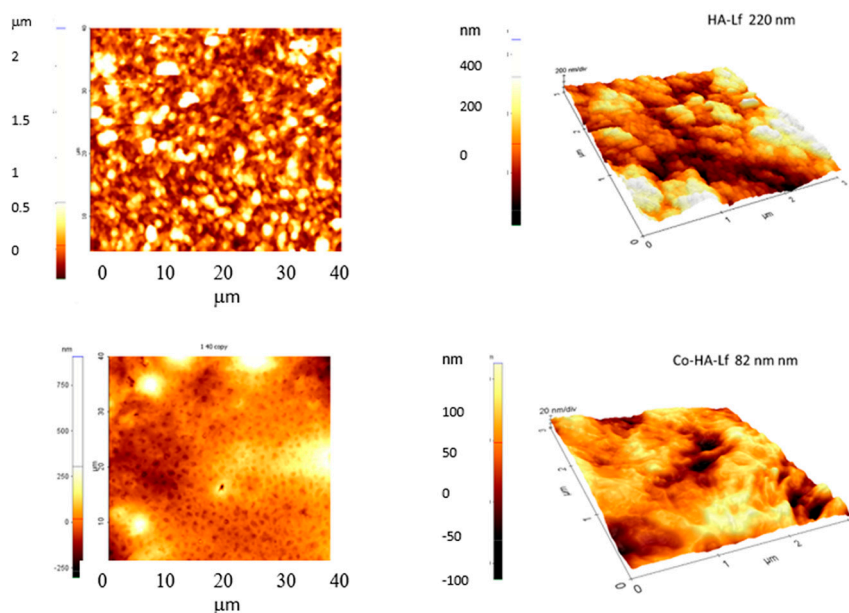


Figure 2. AFM images ($40\ \mu\text{m} \times 40\ \mu\text{m}$) of single component coatings (A) and composite coatings (B). The right column depicts the detailed image of material organization for single component coatings and composite coatings with $5\ \mu\text{m} \times 5\ \mu\text{m}$ and $3\ \mu\text{m} \times 3\ \mu\text{m}$, respectively. HA: hydroxyapatite; Lf: lactoferrin.

The roughness for single components ranged from 217–270 nm, except for Lf which was characterized by a 47 nm roughness, whereas by embedding Lf, HA or both within the polymeric matrix, there was a decrease of up to 118 nm for Co-Lf and only up to 220 nm for HA-Lf. The same tendency of the decrease in roughness of the coating containing the three components was observed (82 nm).

In spite of the differences observed in the surfaces roughness values, the water contact angle measurements were consistent with our previous studies, following the same trend but with slightly small differences in the measured values [58]. Thus, the hydrophilic character of the composite layers Co-Lf, Co-HA, LF-HA, and Co-Lf-HA, as well as of the LF layer, was evidenced by the measured contact angle values of 53° , 64° , 42° , 45° , and 24° , respectively. In the case of single component layer HA, the contact angle was 80° , while for the Co layer, a value of 68° was measured.

3.2. The Behavior of Human THP-1 Cells on Modified Material Surface

During inflammation, monocytes are recruited to the place of implantation where they differentiate toward macrophages. Different culture systems are used to study monocyte/macrophage interaction with biomaterials [67]. In this study, experiments were performed with THP-1 pre-monocytic human cells, a widely used cell line model for inflammation studies [66–70]. THP-1 cells were differentiated to macrophages [71], grown on modified biomimetic surfaces, and their in vitro behavior was analyzed.

3.2.1. Viability and Proliferation of Differentiated Macrophage THP-1 Cells on Modified Material Surface

The proliferation and metabolic activity of the cells attached to and differentiated on the supports were analyzed in the presence and absence of the inflammatory stimulus using the quantitative colorimetric MTS assay. The analysis reflected a directly proportional correlation between the measured absorbance and the number of viable cells. The test revealed a statistically relevant decrease ($p < 0.0001$) in viability in the presence of bacterial endotoxin after 18 h (50 ng/mL LPS) irrespective of the type of surface (Figure 3A). In the absence of lipopolysaccharide, all surfaces analyzed allow cell attachment, with the highest metabolic activity being recorded for cells incubated on the Lf-coated surface. Significantly elevated levels compared to control (uncovered surfaces) were found for THP-1 differentiated cells grown on HA-Lf, Co, Co-HA, Co-HA-Lf coatings ($p < 0.0001$). In the case of LPS treatment, a decrease in metabolic activity compared with the untreated cell was observed.

The viability of the cells attached on the analyzed surfaces was similar, except for those on the Lf and Co-coated surfaces ($p < 0.0001$) and HA-Lf and Co-HA ($p < 0.05$), which promoted survival and an increased cellular proliferation compared to control.

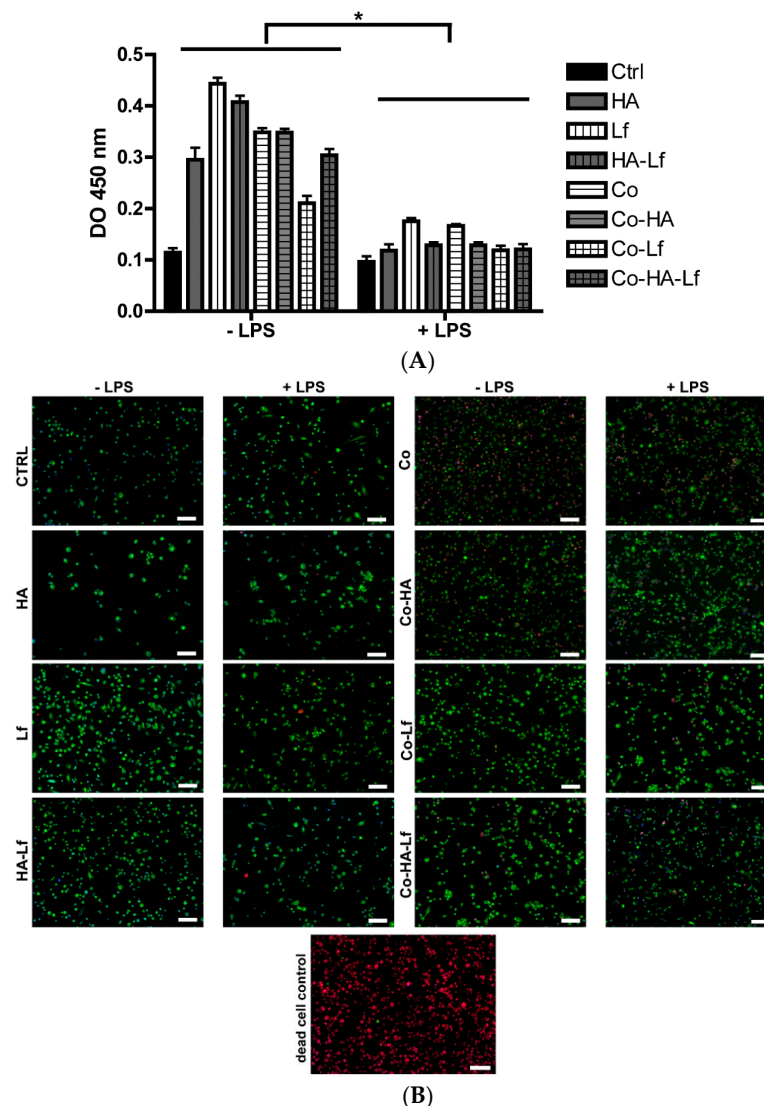


Figure 3. (A) Viability of THP-1 cells attached to surfaces coated with complex hybrid biomimetic components (Co, hydroxyapatite (HA), and lactoferrin (Lf)) in the absence or presence of LPS. Data are presented as mean values \pm SD, and significance was determined at * $p < 0.05$; (B) Fluorescence microscopy images of macrophage-differentiated THP-1 cells on biomimetic modified surfaces (LIVE-DEAD method). The live cells are marked by green fluorescent calcein, and dead cells are labeled with the ethidium-1 homodimer in red. Images of fluorescence microscopy of THP-1 cells adhered for 72 h on the surface of biomaterials and treated or untreated with lipopolysaccharide (LPS) (10 \times). Scale bar 100 μ m.

The LIVE/DEAD assay was subsequently carried out to further verify cell viability using Calcein AM/ethidium-1 homodimer dyes. The method is based on the simultaneous measurement of two parameters, the activity of intracellular esterase and the integrity of the plasma membrane. The ethidium homodimer penetrates the dead cells and binds to the DNA, thus serving as a control for cell death (red cells), while non-fluorescence Calcein AM penetrates through the live cell membrane and, by enzymatic conversion, is transformed into fluorescent calcein, marking the cells green. The results obtained by microscopic investigation of the cells were consistent with those obtained by the MTS method. Fluorescence microscopy images (Figure 3B) showed a decrease in cell number and an increase in

cell death after the treatment with LPS, for almost all types of coatings. The negative effect of LPS stimulation on THP-1 cells survival has also been reported by others [72,73].

3.2.2. Adhesion and Morphology of THP-1 Cells on Modified Material Surface

The cells attach to the surfaces of the materials through a variety of micro extensions, such as filopodia or lamellipodia. In the particular case of macrophages, the interaction with different surfaces involves dynamic cellular adhesion structures [74–76]. Podosomes have an important role in the adhesion and degradation of the cell matrix, as well as in cellular motility [76,77]; these formations being dependent on nature and the characteristics of the substrate. In this study, cellular interaction and morphology were highlighted by fluorescence labeling of actin (green) and vinculin (red) filaments, two proteins of the cellular cytoskeleton involved in cell adhesion. Morphological examination of differentiated macrophage THP-1 cells under standard conditions (without LPS stimulation) indicated a predominantly rounded morphology with smooth edges (Figure 4A) with defined actin and vinculin filaments appearing at the cell peripheral. In the case of Lf-coated surfaces and of those with single or complex Co-coatings, the presence of podosomes suggested an adaptation of morphology to the substrate contact areas. When stimulated with LPS, THP-1 cells showed an increase in cell surface contact with the material. The morphology of the cell was changed and mixed morphologies, spherical, elongated or enlarged surfaces with irregular contours, could be observed (Figure 4B). This morphological behavior might be associated with a cellular activation to the pro-inflammatory phenotype (M1). The cells expressed filopodia and podosome structures that are involved in adhesion and cell motility and might be an adaptation to an external stimulus (LPS), morphology, and surface composition, as it is well known that topographical cues and surface chemistry can influence cellular spreading and the formation of focal adhesion [12,20,78].

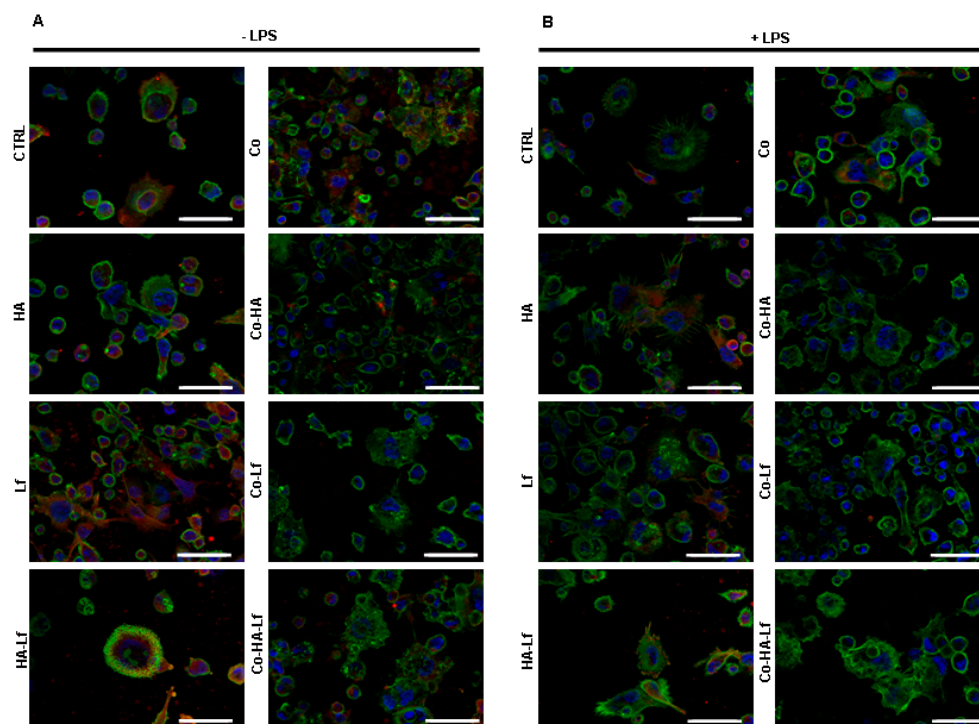


Figure 4. Adhesion and distribution of differentiated THP-1 cells on materials covered with biomimetically modified surfaces in the absence of (A) or in the presence of (B) lipopolysaccharide (LPS). Representative images of the attached cells 40× obtained by fluorescence microscopy by marking actin (green), vinculin (red), and nucleus (blue). Scale bar is 50 μ m. HA: hydroxyapatite; Lf: lactoferrin.

SEM images (Figure 5) taken after macrophage differentiation revealed the presence of spherical cells in the absence of LPS and mixed morphology, an enhancement of cell spread and cell protrusions that allow cell-substrate interactions, in the case of LPS stimulation.

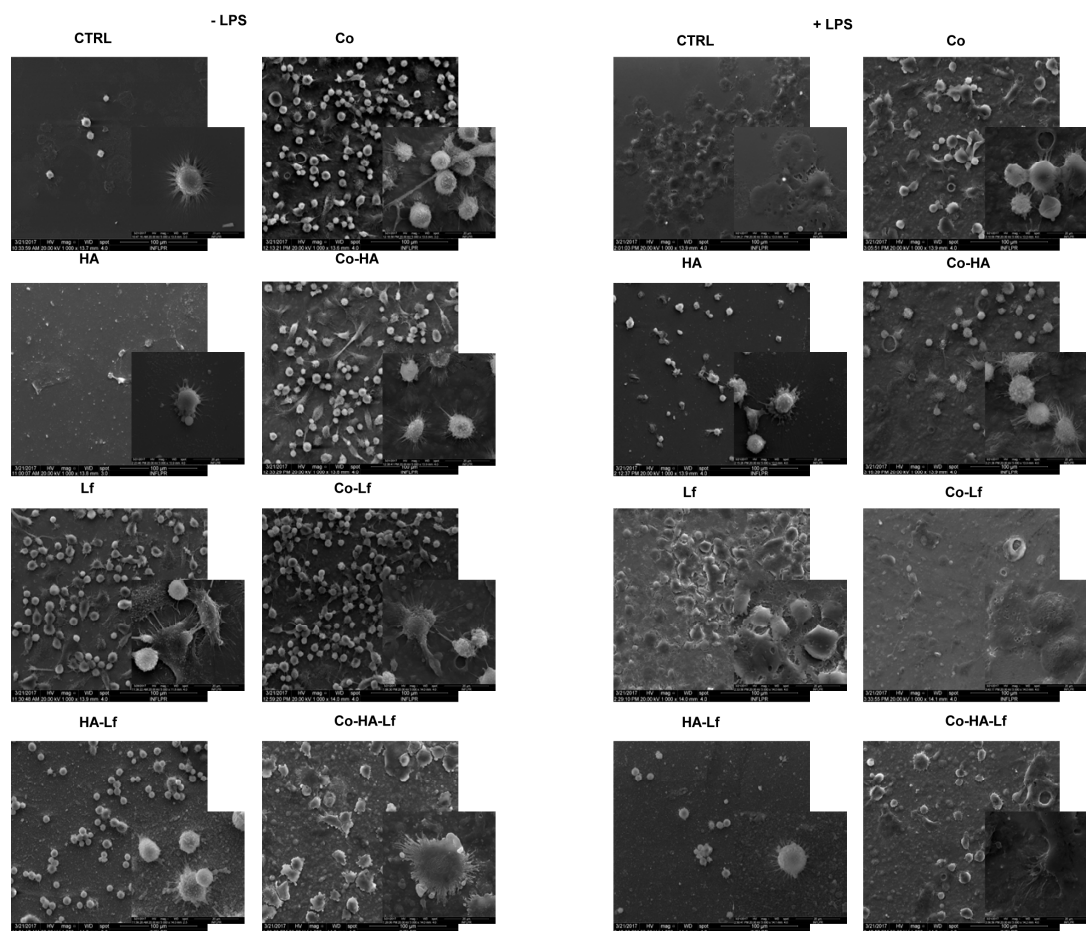


Figure 5. SEM images of THP-1-differentiated macrophages attached to the surface of biomimetically modified surfaces in the absence and presence of bacterial endotoxin. Scale bar 100 µm for 1000× images and 20 µm for the inserted image with 5000× magnification order. HA: hydroxyapatite; Lf: lactoferrin.

3.2.3. Inflammatory Response of THP-1 Cells Grown on Modified Material Surface

To assess the pro-(TNF- α) and anti-inflammatory (IL-10) cytokine secretion, experiments were performed, both under standard culture and inflammatory simulation conditions (LPS treatment), using an ELISA method. The cytokine secretion profile was detected after 18 h, in the absence or presence of the inflammatory stimulus.

TNF- α and IL-10 are two important cytokines, with an immunoregulatory role, expressed by macrophages; TNF- α is associated with the macrophage pro-inflammatory M1 phenotype, while IL-10 cytokine is associated with the M2 anti-inflammatory phenotype [16,21].

No detectable levels of cytokines released by THP-1 cells regardless of the type of surfaces were recorded, suggesting the absence of macrophage activation without LPS treatment. In contrast, treatment with endotoxin led to an increased secretion level of pro-inflammatory and anti-inflammatory cytokines (Figure 6). These findings indicate different cellular activation depending on the physical-chemical characteristics of the coating. The release of TNF- α from macrophages cultured on different surfaces revealed that Lf alone triggered a reduced release of pro-inflammatory cytokine compared to control. However, when the HA component is combined with Lf, the level of cytokine was elevated. The level of TNF- α was also increased, but to a lesser degree, when HA or Lf alone were incorporated into the polymeric matrix (Co). Lf addition within the polymeric matrix together with

the HA component led to a significant reduction ($p < 0.05$) in the release of TNF- α under inflammatory conditions compared to Lf-HA. The capacity of Lf to affect the TNF- α release could be explained by either its ability to directly bind endotoxin, and thus blocking LPS interaction with macrophages, or its capacity to enter macrophages and inhibit pro-inflammatory cytokine production [72,79–81]. In the case of Co-HA-Lf, possible copolymer degradation, previously reported [58], could lead to a reduced level of pro-inflammatory cytokine secreted by macrophages, due to the controlled release of the biological component of the coating.

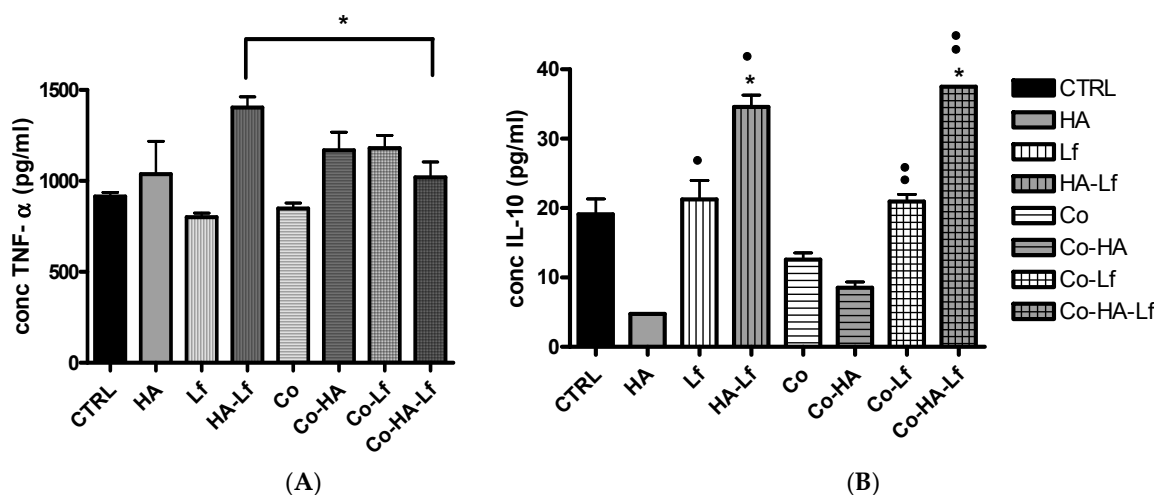


Figure 6. Secreted levels of tumor necrosis factor alpha (TNF- α) (A) and interleukin 10 (IL-10) cytokines (B) normalized to cell activity in lipopolysaccharide (LPS) treated condition. Data are presented as mean values \pm SD, and significance was determined at * $p < 0.05$ vs. CTRL, • $p < 0.05$ vs. HA •• $p < 0.05$ vs. Co-HA. HA: hydroxyapatite; Lf: lactoferrin.

The level of anti-inflammatory IL-10 cytokine released from THP-1 cells seeded on HA-Lf and Co-HA-Lf coatings was notably higher than that released from macrophages cultured on the HA, Co-HA, and Co coatings. Lf and Co-Lf surfaces also induced an increased release of IL-10 from macrophages but to a lesser degree compared to coatings with combined bioactive components. Coatings without Lf seemed to induce the lowest level of anti-inflammatory cytokine release from cells. This behavior could be related to the well-known immune modulatory, anti-inflammatory activity of Lf [82], which counteracts the pro-inflammatory state of macrophages induced by LPS. Also, the increased release of IL-10 from THP-1 cells cultured on HA-Lf and Co-HA-Lf coatings compared with the (rest of) other surfaces could be partially explained by the hydrophobic/hydrophilic character of the coatings. Thus, the IL-10 level measured by ELISA after 18 h of incubation with endotoxin was found to increase with the increase in surface hydrophilicity.

Similarly, Nocerino et al. [54] observed that Lf-HA nanocomposites had an immunomodulatory activity on THP-1 cells stimulated with LPS, decreased the pro-inflammatory cytokines levels, and increased the secretion of anti-inflammatory cytokines.

Knowing that a prolonged release of pro-inflammatory TNF- α cytokine is associated with an inflammatory environment, an osteoclast activation, and alteration of implant integration [83,84], Lf is an important bioactive component that maintains a low inflammatory profile important for proper cellular activation and osteogenic proliferation and differentiation.

Taken together our results suggest that Co-HA-Lf coatings determine a cytokine secretion profile associated with a tissue regeneration-favorable immune response, in agreement with previous data [58], which clearly revealed that the incorporation of HA and Lf into polymeric coating enhanced osteoblastic differentiation.

3.2.4. Surface Effect on Macrophage Polarization

Multiple properties of biomaterial, including physical (topography and roughness) modifications or surface chemistry, can influence immune response and play a significant role in macrophage polarization towards inflammatory M1 or pro-regenerative M2 phenotypes [85–87]. This behavior of macrophages has a direct impact on bone regeneration and biological performance of the biomaterial [88–90]. Different surfaces with diverse chemistry and characteristics control macrophage reaction and phenotype shift [15,91–93], with molecular events and cellular signaling pathways involved in macrophage activation [94]. The cell response differs from the biomaterial surface and in vitro cell models used in the investigation [6,67].

Macrophage polarization induced by surface chemistry and topography correlates with changes in the profile response of cytokine [86]. For studying further the effect of hybrid surfaces on macrophage polarization to the M1 pro-inflammatory phenotype or M2 anti-inflammatory phenotype, the samples were incubated with antibodies specific for membrane markers of classical and alternative activated macrophages. In this case, the presence of a pro-inflammatory phenotypic marker, CCR7, and the anti-inflammatory phenotype specific marker, CD206 [17,95–97], was followed. LPS treatment is a classic polarization protocol to the pro-inflammatory phenotype, but the presence of lactoferrin on the analyzed surfaces, a protein with well-known anti-inflammatory effects, may cause a decrease in the endotoxin effect. Immunomarking of macrophages untreated with inflammatory stimuli revealed a particular activation. The cells displayed characteristics of both M1 and M2 polarization states, especially on coatings with Lf. The cells presented both CCR7 (macrophage M1) and CD206 (macrophage M2) markers on the membrane surface, suggesting that they might be in a state of variable continuing activation between the M1 and M2 state creating a heterogeneous population of macrophages. Representative fluorescent images of the THP-1 cell cultured on different coatings are shown in Figure 7.

This type of behavior was observed as well by Zhang et al. [50,98], who showed that material-activated macrophages do not polarize specifically into M1 or M2 phenotypes but rather are activated into a mixed phenotype with both M1/M2 characteristics.

During the inflammatory process, the macrophages suffer complex activation, expressing the features of both M1 and M2 phenotypes. This activation could explain the simultaneous expression of M1/M2 specific markers, the secretion of both pro and anti-inflammatory cytokines, as well as the presence of mixed cell morphologies on composite surfaces. In the case of endotoxin stimulation, it seemed that Lf counteracted the inflammatory effect induced by LPS, while the cells cultured on coatings with Lf alone or in combination with HA or copolymer displayed an enhanced anti-inflammatory M2 phenotype expression marker CD206 on the cell surface. The results could be correlated with the ability of Lf to modulate the polarization of macrophages through its anti-inflammatory properties [82] and also with the hydrophilic character of the hybrid coating [14]. In addition, M1-to-M2 transition on hybrid coatings of THP-1 cells stimulated with LPS could also be explained by the interference of the hydroxyapatite component [99,100] and the polymeric coating, which might be involved in a controlled release of the anti-inflammatory component [58].

Besides chemical-structural characteristics of our materials with anti-inflammatory effects (Lf, HA), the roughness could have also an impact on macrophage polarization. Generally, surface roughness maintained in the nanometer scale induces a decrease in M1 development of macrophages and an increase in M2 phenotype [101]. Our films generated by each condition exhibited a submicron roughness, with lowest values for coatings containing Lf alone or embedded within the polymeric matrix. These films exhibited increased levels of anti-inflammatory IL-10 and the increased polarization of THP-1 cells towards an M2 phenotype.

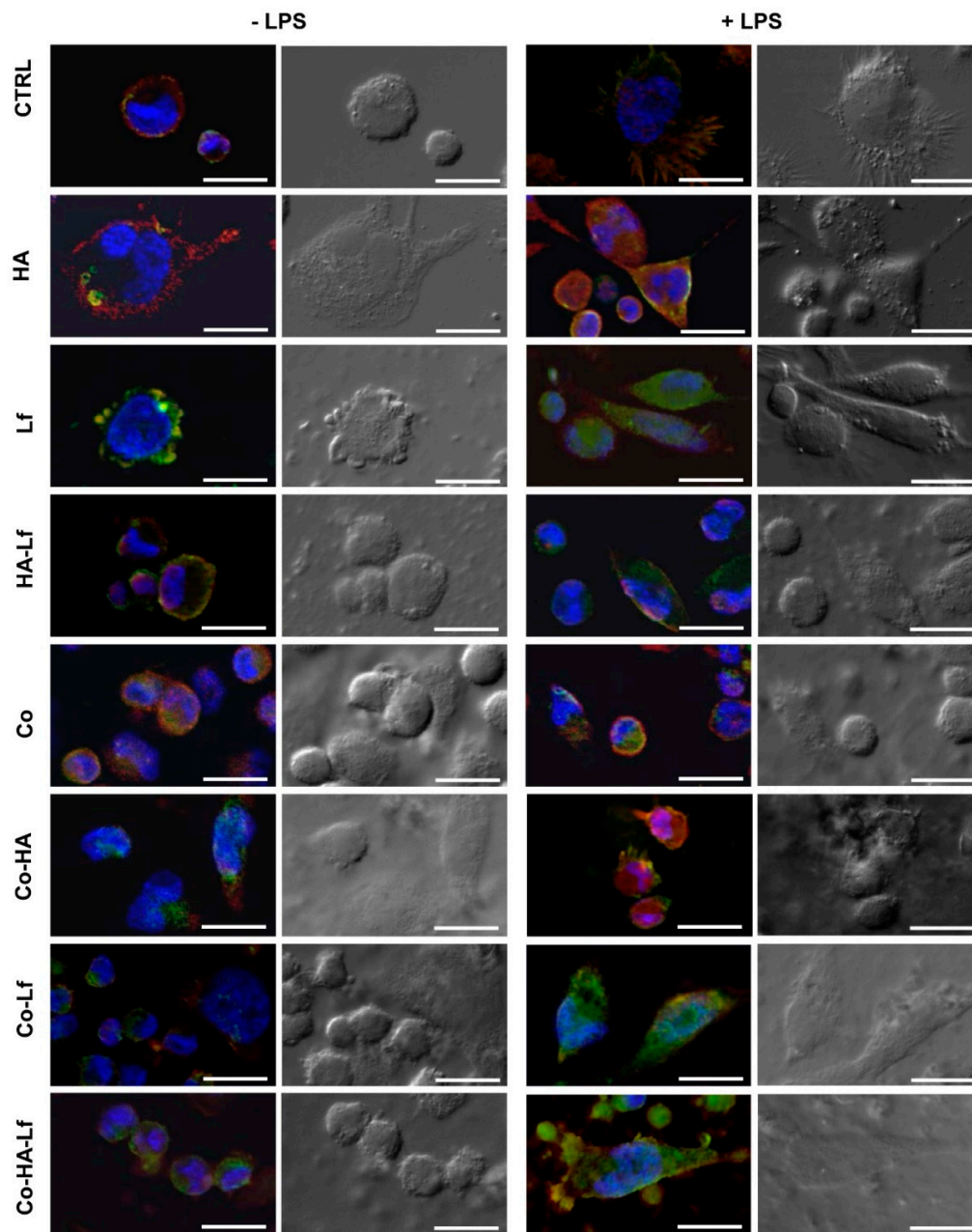


Figure 7. The polarization of differentiated THP-1 cells on biomimetic coatings. Immunofluorescence images (40×) of CCR7 M1 markers (red), CD206 M2 (green) on the cell surface, and nucleus (blue) in the absence (left) and in the presence of (right) lipopolysaccharide (LPS) (Columns 1 and 3). Associated images of optical microscopy (Columns 2 and 4). Scale bar 20 μ m. HA: hydroxyapatite; Lf: lactoferrin.

4. Conclusions

The results revealed that the use of a Copolymer-HA-Lf composite could be a promising approach to the creation of coatings for bone implant materials. In the presence of an LPS stimulus, surfaces exhibited low levels of pro-inflammatory $\text{TNF-}\alpha$, increased levels of anti-inflammatory IL-10, and the increased polarization of THP-1 cells towards an M2 pro-reparative phenotype. Controlled release of the components by polymeric coating allowed the combination of the properties of the two biological compounds, namely the osteogenic capacity and bone mechanical stability of HA with the anti-inflammatory and osteogenic effect of the Lf component, making the composition excellent support for bone regeneration.

Author Contributions: Conceptualization, M.I., A.R., and V.D.; Methodology, M.I., L.R., S.B., A.B., A.R., and V.D.; Validation, M.I., L.R.; Formal Analysis, M.I., V.D.; Investigation, M.I., L.R., S.B., A.B., and V.D.; Resources, V.D., M.I., and A.R.; Writing—Original Draft Preparation, M.I., V.D.; Writing—Review and Editing, A.R., R.W.E., M.D., and A.C.; Supervision, A.R., R.W.E., and A.C.

Funding: This research received funding from Romanian National Authority for Scientific Research (CNCS-UEFISCDI), under the projects TERAMED 63PCCDI/2018, PN-III-P1-1.2-PCCDI-2017-072 and Nucleu 16N/08.02.2019, Structural and Functional Proteomics Research Program of the Institute of Biochemistry of the Romanian Academy, and by the University of Bucharest-Biology Doctoral School.

Conflicts of Interest: The authors declare no conflict of interest.

References

- Gordon, S.; Taylor, P.R. Monocyte and macrophage heterogeneity. *Nat. Rev. Immunol.* **2005**, *5*, 953–964. [[CrossRef](#)] [[PubMed](#)]
- Gordon, S.; Martinez, F.O. Alternative Activation of Macrophages: Mechanism and Functions. *Immunity* **2010**, *32*, 593–604. [[CrossRef](#)] [[PubMed](#)]
- Koh, T.J.; DiPietro, L.A. Inflammation and wound healing: the role of the macrophage. *Expert. Rev. Mol. Med.* **2011**, *13*, e23. [[CrossRef](#)]
- Sica, A.; Mantovani, A. Macrophage plasticity and polarization: in vivo veritas. *J. Clin. Invest.* **2012**, *122*, 787–795. [[CrossRef](#)] [[PubMed](#)]
- Gaffney, L.; Warren, P.; Wrona, E.A.; Fisher, M.B.; Freytes, D.O. Macrophages' Role in Tissue Disease and Regeneration. *Results Probl. Cell. D* **2017**, *62*, 245–271.
- Rayahin, J.E.; Gemeinhart, R.A. Activation of Macrophages in Response to Biomaterials. *Results Probl. Cell. D* **2017**, *62*, 317–351.
- Luttikhuisen, D.T.; Harmsen, M.C.; Van Luyn, M.J.A. Cellular and molecular dynamics in the foreign body reaction. *Tissue. Eng.* **2006**, *12*, 1955–1970. [[CrossRef](#)] [[PubMed](#)]
- Anderson, J.M.; Rodriguez, A.; Chang, D.T. Foreign body reaction to biomaterials. *Semin. Immunol.* **2008**, *20*, 86–100. [[CrossRef](#)] [[PubMed](#)]
- Franz, S.; Rammelt, S.; Scharnweber, D.; Simon, J.C. Immune responses to implants—A review of the implications for the design of immunomodulatory biomaterials. *Biomaterials* **2011**, *32*, 6692–6709. [[CrossRef](#)]
- Ogle, M.E.; Segar, C.E.; Sridhar, S.; Botchwey, E.A. Monocytes and macrophages in tissue repair: Implications for immunoregenerative biomaterial design. *Exp. Biol. Med.* **2016**, *241*, 1084–1097. [[CrossRef](#)] [[PubMed](#)]
- Bartneck, M.; Schulte, V.A.; Paul, N.E.; Diez, M.; Lensen, M.C.; Zwadlo-Klarwasser, G. Induction of specific macrophage subtypes by defined micro-patterned structures. *Acta Biomaterialia* **2010**, *6*, 3864–3872. [[CrossRef](#)] [[PubMed](#)]
- McWhorter, F.Y.; Wang, T.T.; Nguyen, P.; Chung, T.; Liu, W.F. Modulation of macrophage phenotype by cell shape. *P Natl. Acad. Sci. USA* **2013**, *110*, 17253–17258. [[CrossRef](#)]
- Singh, S.; Awuah, D.; Rostam, H.M.; Emes, R.D.; Kandola, N.K.; Onion, D.; Htwe, S.S.; Rajchagool, B.; Cha, B.H.; Kim, D.; et al. Unbiased Analysis of the Impact of Micropatterned Biomaterials on Macrophage Behavior Provides Insights beyond Predefined Polarization States. *ACS. Biomater. Sci. Eng.* **2017**, *3*, 969–978. [[CrossRef](#)]
- Lv, L.; Xie, Y.T.; Li, K.; Hu, T.; Lu, X.; Cao, Y.Z.; Zheng, X.B. Unveiling the Mechanism of Surface Hydrophilicity-Modulated Macrophage Polarization. *Adv. Healthc. Mater.* **2018**, *7*, 1800675. [[CrossRef](#)] [[PubMed](#)]
- Hotchkiss, K.M.; Reddy, G.B.; Hyzy, S.L.; Schwartz, Z.; Boyan, B.D.; Olivares-Navarrete, R. Titanium surface characteristics, including topography and wettability, alter macrophage activation. *Acta. Biomaterialia* **2016**, *31*, 425–434. [[CrossRef](#)] [[PubMed](#)]
- Mosser, D.M.; Edwards, J.P. Exploring the full spectrum of macrophage activation. *Nat. Rev. Immunol.* **2008**, *8*, 958–969. [[CrossRef](#)] [[PubMed](#)]
- Martinez, F.O.; Helming, L.; Gordon, S. Alternative Activation of Macrophages: An Immunologic Functional Perspective. *Annu. Rev. Immunol.* **2009**, *27*, 451–483. [[CrossRef](#)]
- Brown, B.N.; Goodman, S.B.; Amar, S.; Badylak, S.F. Macrophage polarization: an opportunity for improved outcomes in biomaterials and regenerative medicine. *Biomaterials* **2012**, *33*, 3792–3802. [[CrossRef](#)]

19. Brown, B.N.; Badylak, S.F. Expanded applications, shifting paradigms and an improved understanding of host–biomaterial interactions. *Acta. Biomaterialia* **2013**, *9*, 4948–4955. [\[CrossRef\]](#)
20. Lee, H.S.; Stachelek, S.J.; Tomczyk, N.; Finley, M.J.; Composto, R.J.; Eckmann, D.M. Correlating macrophage morphology and cytokine production resulting from biomaterial contact. *J. Biomed. Mater. Res. A* **2013**, *101*, 203–212. [\[CrossRef\]](#)
21. Murray, P.J.; Allen, J.E.; Biswas, S.K.; Fisher, E.A.; Gilroy, D.W.; Goerdt, S.; Gordon, S.; Hamilton, J.A.; Ivashkiv, L.B.; Lawrence, T.; et al. Macrophage Activation and Polarization: Nomenclature and Experimental Guidelines. *Immunity* **2014**, *41*, 339–340. [\[CrossRef\]](#)
22. Martinez, F.O.; Gordon, S. The M1 and M2 paradigm of macrophage activation: Time for reassessment. *F1000Prime Rep.* **2014**, *6*, 13. [\[CrossRef\]](#)
23. Italiani, P.; Boraschi, D. From monocytes to M1/M2 macrophages: Phenotypical vs. functional differentiation. *Front. Immunol.* **2014**. [\[CrossRef\]](#)
24. He, X.-T.; Li, X.; Xia, Y.; Yin, Y.; Wu, R.-X.; Sun, H.-H.; Chen, F.-M. Building capacity for macrophage modulation and stem cell recruitment in high-stiffness hydrogels for complex periodontal regeneration: Experimental studies in vitro and in rats. *Acta. Biomater.* **2019**, *88*, 162–180. [\[CrossRef\]](#)
25. Wu, R.X.; Xu, X.Y.; Wang, J.; He, X.T.; Sun, H.H.; Chen, F.M. Biomaterials for endogenous regenerative medicine: Coaxing stem cell homing and beyond. *Appl. Mater. Today* **2018**, *11*, 144–165. [\[CrossRef\]](#)
26. Yu, Y.; Wu, R.X.; Yin, Y.; Chen, F.M. Directing immunomodulation using biomaterials for endogenous regeneration. *J. Mater. Chem. B* **2016**, *4*, 569–584. [\[CrossRef\]](#)
27. Lee, J.; Byun, H.; Madhurakkat Perikamana, S.K.; Lee, S.; Shin, H. Current Advances in Immunomodulatory Biomaterials for Bone Regeneration. *Adv. Healthc. Mater.* **2018**, *8*, 1801106. [\[CrossRef\]](#)
28. Chen, Z.T.; Klein, T.; Murray, R.Z.; Crawford, R.; Chang, J.; Wu, C.T.; Xiao, Y. Osteoimmunomodulation for the development of advanced bone biomaterials. *Mater. Today* **2016**, *19*, 304–321. [\[CrossRef\]](#)
29. Zhou, G.Y.; Groth, T. Host Responses to Biomaterials and Anti-Inflammatory Design—A Brief Review. *Macromol. Biosci.* **2018**, *18*, 1800112. [\[CrossRef\]](#)
30. Andorko, J.I.; Jewell, C.M. Designing biomaterials with immunomodulatory properties for tissue engineering and regenerative medicine. *Bioeng. Transl. Med.* **2017**, *2*, 139–155. [\[CrossRef\]](#)
31. Nagano-Takebe, F.; Miyakawa, H.; Nakazawa, F.; Endo, K. Inhibition of initial bacterial adhesion on titanium surfaces by lactoferrin coating. *Biointerphases* **2014**, *9*, 029006. [\[CrossRef\]](#)
32. Etheridge, M.L.; Campbell, S.A.; Erdman, A.G.; Haynes, C.L.; Wolf, S.M.; McCullough, J. The big picture on nanomedicine: the state of investigational and approved nanomedicine products. *Nanomed. Nanotechnol. Biol. Med.* **2013**, *9*, 1–14. [\[CrossRef\]](#) [\[PubMed\]](#)
33. Tang, H.; Zhao, W.; Yu, J.; Li, Y.; Zhao, C. Recent Development of pH-Responsive Polymers for Cancer Nanomedicine. *Molecules* **2018**, *24*, 4. [\[CrossRef\]](#) [\[PubMed\]](#)
34. Grossen, P.; Witzigmann, D.; Sieber, S.; Huwyler, J. PEG-PCL-based nanomedicines: A biodegradable drug delivery system and its application. *J. Control. Release* **2017**, *260*, 46–60. [\[CrossRef\]](#) [\[PubMed\]](#)
35. Zhang, K.; Wang, S.; Zhou, C.; Cheng, L.; Gao, X.; Xie, X.; Sun, J.; Wang, H.; Weir, M.D.; Reynolds, M.A.; et al. Advanced smart biomaterials and constructs for hard tissue engineering and regeneration. *Bone Res.* **2018**, *6*, 31. [\[CrossRef\]](#) [\[PubMed\]](#)
36. Moreno-Exposito, L.; Illescas-Montes, R.; Melguizo-Rodriguez, L.; Ruiz, C.; Ramos-Torrecillas, J.; de Luna-Bertos, E. Multifunctional capacity and therapeutic potential of lactoferrin. *Life Sci.* **2018**, *195*, 61–64. [\[CrossRef\]](#) [\[PubMed\]](#)
37. Garcia-Montoya, I.A.; Cendon, T.S.; Arevalo-Gallegos, S.; Rascon-Cruz, Q. Lactoferrin a multiple bioactive protein: An overview. *Bba-Gen Subjects* **2012**, *1820*, 226–236. [\[CrossRef\]](#)
38. Legrand, D.; Ellass, E.; Pierce, A.; Mazurier, J. Lactoferrin and host defence: An overview of its immuno-modulating and anti-inflammatory properties. *Biomaterials* **2004**, *17*, 225–229. [\[CrossRef\]](#)
39. Legrand, D.; Ellass, E.; Carpentier, M.; Mazurier, J. Lactoferrin: A modulator of immune and inflammatory responses. *Cell. Mol. Life Sci.* **2005**, *62*, 2549. [\[CrossRef\]](#)
40. Legrand, D.; Ellass, E.; Carpentier, M.; Mazurier, J. Interactions of lactoferrin with cells involved in immune function. *Biochem. Cell Biol.* **2006**, *84*, 282–290. [\[CrossRef\]](#)
41. Suzuki, Y.A.; Lopez, V.; Lonnerdal, B. Mammalian lactoferrin receptors: Structure and function. *Cell. Mol. Life Sci.* **2005**, *62*, 2560–2575. [\[CrossRef\]](#) [\[PubMed\]](#)

42. Legrand, D.; Mazurier, J. A critical review of the roles of host lactoferrin in immunity. *BioMetals* **2010**, *23*, 365–376. [[CrossRef](#)] [[PubMed](#)]
43. Legrand, D. Lactoferrin, a key molecule in immune and inflammatory processes. *Biochem. Cell Biol.* **2011**, *90*, 252–268. [[CrossRef](#)] [[PubMed](#)]
44. Legrand, D. Overview of Lactoferrin as a Natural Immune Modulator. *J. Pediatrics* **2016**, *173*, S10–S15. [[CrossRef](#)] [[PubMed](#)]
45. Cornish, J.; Callon, K.E.; Naot, D.; Palmano, K.P.; Banovic, T.; Bava, U.; Watson, M.; Lin, J.M.; Tong, P.C.; Chen, Q.; et al. Lactoferrin is a potent regulator of bone cell activity and increases bone formation in vivo. *Endocrinology* **2004**, *145*, 4366–4374. [[CrossRef](#)]
46. Cornish, J.; Palmano, K.; Callon, K.E.; Watson, M.; Lin, J.M.; Valenti, P.; Naot, D.; Grey, A.B.; Reid, I.R. Lactoferrin and bone; structure–activity relationships. *Biochem. Cell Biol.* **2006**, *84*, 297–302. [[CrossRef](#)]
47. Cornish, J.; Naot, D. Lactoferrin as an effector molecule in the skeleton. *Biomaterials* **2010**, *23*, 425–430. [[CrossRef](#)]
48. Rydén, L.; Omar, O.; Johansson, A.; Jimbo, R.; Palmquist, A.; Thomsen, P. Inflammatory cell response to ultra-thin amorphous and crystalline hydroxyapatite surfaces. *J. Mater. Sci.: Mater. Med.* **2016**, *28*, 9.
49. Mestres, G.; Espanol, M.; Xia, W.; Persson, C.; Ginebra, M.P.; Ott, M.K. Inflammatory Response to Nano- and Microstructured Hydroxyapatite. *Plos One* **2015**, *10*, e0120381. [[CrossRef](#)]
50. Zhang, Y.; Cheng, X.; Jansen, J.A.; Yang, F.; van den Beucken, J.J.J.P. Titanium surfaces characteristics modulate macrophage polarization. *Mat. Sci. Eng. C–Mater.* **2019**, *95*, 143–151. [[CrossRef](#)]
51. Montesi, M.; Panseri, S.; Iafisco, M.; Adamiano, A.; Tampieri, A. Coupling Hydroxyapatite Nanocrystals with Lactoferrin as a Promising Strategy to Fine Regulate Bone Homeostasis. *PloS ONE* **2015**, *10*, e0132633. [[CrossRef](#)] [[PubMed](#)]
52. Montesi, M.; Panseri, S.; Iafisco, M.; Adamiano, A.; Tampieri, A. Effect of hydroxyapatite nanocrystals functionalized with lactoferrin in osteogenic differentiation of mesenchymal stem cells. *J. Biomed. Mater. Res. A* **2015**, *103*, 224–234. [[CrossRef](#)] [[PubMed](#)]
53. Fulgione, A.; Nocerino, N.; Iannaccone, M.; Roperto, S.; Capuano, F.; Roveri, N.; Lelli, M.; Crasto, A.; Calogero, A.; Piloni, A.P.; et al. Lactoferrin Adsorbed onto Biomimetic Hydroxyapatite Nanocrystals Controlling—In Vivo—the *Helicobacter pylori* Infection. *Plos ONE* **2016**, *11*, e0158646. [[CrossRef](#)]
54. Nocerino, N.; Fulgione, A.; Iannaccone, M.; Tomasetta, L.; Ianniello, F.; Martora, F.; Lelli, M.; Roveri, N.; Capuano, F.; Capparelli, R. Biological activity of lactoferrin- functionalized biomimetic hydroxyapatite nanocrystals. *Int. J. Nanomed.* **2014**, *9*, 1175–1184.
55. Bhushan, B.; Schricker, S.R. A review of block copolymer-based biomaterials that control protein and cell interactions. *J. Biomed. Mater. Res. A* **2014**, *102*, 2467–2480. [[CrossRef](#)] [[PubMed](#)]
56. Fan, Y.Q.; Li, X.; Yang, R.J. The Surface Modification Methods for Constructing Polymer-Coated Stents. *Int. J. Polym. Sci.* **2018**. [[CrossRef](#)]
57. Dinca, V.; Florian, P.E.; Sima, L.E.; Rusen, L.; Constantinescu, C.; Evans, R.W.; Dinescu, M.; Roseanu, A. MAPLE-based method to obtain biodegradable hybrid polymeric thin films with embedded antitumoral agents. *Biomed. Microdevices* **2014**, *16*, 11–21. [[CrossRef](#)]
58. Rusen, L.; Brajnicov, S.; Neacsu, P.; Marascu, V.; Bonciu, A.; Dinescu, M.; Dinca, V.; Cimpean, A. Novel degradable biointerfacing nanocomposite coatings for modulating the osteoblast response. *Surf. Coat. Tech.* **2017**, *325*, 397–409. [[CrossRef](#)]
59. Dinca, V.; Viespe, C.; Brajnicov, S.; Constantinoiu, I.; Moldovan, A.; Bonciu, A.; Toader, C.N.; Ginghina, R.E.; Grigoriu, N.; Dinescu, M.; et al. MAPLE Assembled Acetylcholinesterase-Polyethylenimine Hybrid and Multilayered Interfaces for Toxic Gases Detection. *Sensors* **2018**, *18*, 4265. [[CrossRef](#)]
60. Pique, A.; Chrisey, D.B.; Spargo, B.J.; Bucaro, M.A.; Vachet, R.W.; Callahan, J.H.; McGill, R.A.; Leonhardt, D.; Mlsna, T.E. Use of matrix assisted pulsed laser evaporation (MAPLE) for the growth of organic thin films. *Mater. Res. Soc. Symp. P* **1998**, *526*, 421–426. [[CrossRef](#)]
61. Sima, F.; Davidson, P.; Pauthe, E.; Sima, L.E.; Gallet, O.; Mihailescu, I.N.; Anselme, K. Fibronectin layers by matrix-assisted pulsed laser evaporation from saline buffer-based cryogenic targets. *Acta. Biomater.* **2011**, *7*, 3780–3788. [[CrossRef](#)]
62. Caricato, A.P.; Luches, A. Applications of the matrix-assisted pulsed laser evaporation method for the deposition of organic, biological and nanoparticle thin films: A review. *Appl. Phys. Mater.* **2011**, *105*, 565–582. [[CrossRef](#)]

63. McGill, R.A.; Chrisey, D.B.; Pique, A.; Mlsna, T.E. Matrix-assisted pulsed-laser evaporation (MAPLE) of functionalized polymers: Applications with chemical sensors. *SPIE* **1998**, 3274, 12.
64. Constantinescu, C.; Matei, A.; Ionita, I.; Ion, V.; Marascu, V.; Dinescu, M.; Vasiliu, I.C.; Emandi, A. Azo-derivatives thin films grown by matrix-assisted pulsed laser evaporation for nonlinear optical applications. *Appl. Surf. Sci.* **2014**, 302, 69–73. [\[CrossRef\]](#)
65. Ion, V.; Matei, A.; Constantinescu, C.; Ionita, I.; Marinescu, A.; Dinescu, M.; Emandi, A. Octahydroacridine thin films grown by matrix-assisted pulsed laser evaporation for non linear optical applications. *Mat. Sci. Semicon. Proc.* **2015**, 36, 78. [\[CrossRef\]](#)
66. Ward, P.P.; Uribe-Luna, S.; Conneely, O.M. Lactoferrin and host defense. *Biochem Cell Biol* **2002**, 80, 95–102. [\[CrossRef\]](#)
67. Boersema, G.S.A.; Grotenhuis, N.; Bayon, Y.; Lange, J.F.; Bastiaansen-Jenniskens, Y.M. The Effect of Biomaterials Used for Tissue Regeneration Purposes on Polarization of Macrophages. *BioResearch Open Acc* **2016**, 5, 6–14. [\[CrossRef\]](#)
68. Auwerx, J. The Human Leukemia-Cell Line, Thp-1—A Multifaceted Model for the Study of Monocyte-Macrophage Differentiation. *Experientia* **1991**, 47, 22–31. [\[CrossRef\]](#)
69. Park, E.K.; Jung, H.S.; Yang, H.I.; Yoo, M.C.; Kim, C.; Kim, K.S. Optimized THP-1 differentiation is required for the detection of responses to weak stimuli. *Inflamm. Res.* **2007**, 56, 45–50. [\[CrossRef\]](#)
70. Chanput, W.; Mes, J.J.; Savelkoul HF, J.; Wichers, H.J. Characterization of polarized THP-1 macrophages and polarizing ability of LPS and food compounds. *Food Funct.* **2013**, 4, 266–276. [\[CrossRef\]](#)
71. Lund, M.E.; To, J.; O'Brien, B.A.; Donnelly, S. The choice of phorbol 12-myristate 13-acetate differentiation protocol influences the response of THP-1 macrophages to a pro-inflammatory stimulus. *J. Immunol. Methods* **2016**, 430, 64–70. [\[CrossRef\]](#)
72. Choe, Y.H.; Lee, S.W. Effect of lactoferrin on the production of tumor necrosis factor-alpha and nitric oxide. *J. Cell Biochem.* **2000**, 76, 30–36. [\[CrossRef\]](#)
73. Starr, T.; Bauler, T.J.; Malik-Kale, P.; Steele-Mortimer, O. The phorbol 12-myristate-13-acetate differentiation protocol is critical to the interaction of THP-1 macrophages with Salmonella Typhimurium. *PLoS ONE* **2018**, 13, e0193601. [\[CrossRef\]](#)
74. Linder, S.; Aepfelbacher, M. Podosomes: Adhesion hot-spots of invasive cells. *Trends Cell Biol.* **2003**, 13, 376–385. [\[CrossRef\]](#)
75. Linder, S.; Wiesner, C. Tools of the trade: Podosomes as multipurpose organelles of monocytic cells. *Cell. Mol. Life Sci.* **2015**, 72, 121–135. [\[CrossRef\]](#)
76. Gimona, M.; Buccione, R.; Courtneidge, S.A.; Linder, S. Assembly and biological role of podosomes and invadopodia. *Curr. Opin. Cell Biol.* **2008**, 20, 235–241. [\[CrossRef\]](#)
77. Linder, S. The matrix corroded: Podosomes and invadopodia in extracellular matrix degradation. *Trends. Cell Biol.* **2007**, 17, 107–117. [\[CrossRef\]](#)
78. Rammal, H.; Bour, C.; Dubus, M.; Entz, L.; Aubert, L.; Gangloff, S.C.; Audonnet, S.; Bercu, N.B.; Boulmedais, F.; Mauprivez, C.; et al. Combining Calcium Phosphates with Polysaccharides: A Bone-Inspired Material Modulating Monocyte/Macrophage Early Inflammatory Response. *Int. J. Mol. Sci.* **2018**, 19, 3458. [\[CrossRef\]](#)
79. Puddu, P.; Latorre, D.; Valenti, P.; Gessani, S. Immunoregulatory role of lactoferrin-lipopolysaccharide interactions. *Biometals* **2010**, 23, 387–397. [\[CrossRef\]](#)
80. Ellass-Rochard, E.; Legrand, D.; Salmon, V.; Roseanu, A.; Trif, M.; Tobias, P.S.; Mazurier, J.; Spik, G. Lactoferrin inhibits the endotoxin interaction with CD14 by competition with the lipopolysaccharide-binding protein. *Infect. Immun.* **1998**, 66, 486–491.
81. Haversen, L.; Ohlsson, B.G.; Hahn-Zoric, M.; Hanson, L.A.; Mattsby-Baltzer, I. Lactoferrin down-regulates the LPS-induced cytokine production in monocytic cells via NF-kappa B. *Cell Immunol.* **2002**, 220, 83–95. [\[CrossRef\]](#)
82. Cutone, A.; Rosa, L.; Lepanto, M.S.; Scotti, M.J.; Berlutti, F.; di Patti, M.C.B.; Musci, G.; Valenti, P. Lactoferrin Efficiently Counteracts the Inflammation-Induced Changes of the Iron Homeostasis System in Macrophages. *Front. Immunol.* **2017**, 8, 705. [\[CrossRef\]](#)
83. Boyce, B.E.; Li, P.; Yao, Z.; Zhang, Q.; Badell, I.R.; Schwarz, E.M.; Keefe, R.J.; Xing, L. TNF α and pathologic bone resorption. *Keio J. Med.* **2005**, 54, 127–131. [\[CrossRef\]](#)
84. Zhao, B.H.; Grimes, S.N.; Li, S.S.; Hu, X.Y.; Ivashkiv, L.B. TNF-induced osteoclastogenesis and inflammatory bone resorption are inhibited by transcription factor RBP-J. *J. Exp. Med.* **2012**, 209, 319–334. [\[CrossRef\]](#)

85. Rostam, H.M.; Singh, S.; Salazar, F.; Magennis, P.; Hook, A.; Singh, T.; Vrana, N.E.; Alexander, M.R.; Ghaemmaghami, A.M. The impact of surface chemistry modification on macrophage polarisation. *Immunobiology* **2016**, *221*, 1237–1246. [\[CrossRef\]](#)
86. Sridharan, R.; Cameron, A.R.; Kelly, D.J.; Kearney, C.J.; O'Brien, F.J. Biomaterial based modulation of macrophage polarization: A review and suggested design principles. *Mater. Today* **2015**, *18*, 313–325. [\[CrossRef\]](#)
87. Luu, T.U.; Gott, S.C.; Woo BW, K.; Rao, M.P.; Liu, W.F. Micro- and Nanopatterned Topographical Cues for Regulating Macrophage Cell Shape and Phenotype. *ACS Appl. Mater. Interfaces* **2015**, *7*, 28665–28672. [\[CrossRef\]](#)
88. Wang, J.; Meng, F.; Song, W.; Jin, J.; Ma, Q.; Fei, D.; Fang, L.; Chen, L.; Wang, Q.; Zhang, Y. Nanostructured titanium regulates osseointegration via influencing macrophage polarization in the osteogenic environment. *Int. J. Nanomed.* **2018**, *13*, 4029–4043. [\[CrossRef\]](#)
89. Nassiri, S.; Graney, P.; Spiller, K.L. Manipulation of Macrophages to Enhance Bone Repair and Regeneration. In *A Tissue Regeneration Approach to Bone and Cartilage Repair*; Zreiqat, H., Dunstan, C.R., Rosen, V., Eds.; Springer International Publishing: Cham, Switzerland, 2015; pp. 65–84.
90. Ma, Q.-L.; Zhao, L.-Z.; Liu, R.-R.; Jin, B.-Q.; Song, W.; Wang, Y.; Zhang, Y.-S.; Chen, L.-H.; Zhang, Y.-M. Improved implant osseointegration of a nanostructured titanium surface via mediation of macrophage polarization. *Biomaterials* **2014**, *35*, 9853–9867. [\[CrossRef\]](#)
91. Chung, L.; Maestas, D.R.; Housseau, F.; Elisseeff, J.H. Key players in the immune response to biomaterial scaffolds for regenerative medicine. *Adv. Drug. Deliv. Rev.* **2017**, *114*, 184–192. [\[CrossRef\]](#)
92. Fernandes, K.R.; Zhang, Y.; Magri, A.M.P.; Renno, A.C.M.; van den Beucken, J.J.J.P. Biomaterial Property Effects on Platelets and Macrophages: An *in Vitro* Study. *ACS Biomater. Sci. Eng.* **2017**, *3*, 3318–3327. [\[CrossRef\]](#)
93. Chen, Z.; Bachhuka, A.; Han, S.; Wei, F.; Lu, S.; Visalakshan, R.M.; Vasilev, K.; Xiao, Y. Tuning Chemistry and Topography of Nanoengineered Surfaces to Manipulate Immune Response for Bone Regeneration Applications. *ACS Nano* **2017**, *11*, 4494–4506. [\[CrossRef\]](#)
94. Moore, L.B.; Kyriakides, T.R. Immune Responses to Biosurfaces. In *Molecular Characterization of Macrophage-Biomaterial Interactions*; Lambris, J.D., Ekdahl, K.N., Ricklin, D., Nilsson, B., Eds.; Springer International Publishing: Cham, Switzerland, 2015; pp. 109–122.
95. Van Ginderachter, J.A.; Movahedi, K.; Ghassabeh, G.H.; Meerschaut, S.; Beschin, A.; Raes, G.; De Baetselier, P. Classical and alternative activation of mononuclear phagocytes: Picking the best of both worlds for tumor promotion. *Immunobiology* **2006**, *211*, 487–501. [\[CrossRef\]](#)
96. Joshi, A.D.; Oak, S.R.; Hartigan, A.J.; Finn, W.G.; Kunkel, S.L.; Duffy, K.E.; Das, A.; Hogaboam, C.M. Interleukin-33 contributes to both M1 and M2 chemokine marker expression in human macrophages. *Bmc. Immunol* **2010**, *11*, 52. [\[CrossRef\]](#)
97. Miao, X.C.; Wang, D.H.; Xu, L.Y.; Wang, J.; Zeng, D.L.; Lin, S.X.; Huang, C.; Liu, X.Y.; Jiang, X.Q. The response of human osteoblasts, epithelial cells, fibroblasts, macrophages and oral bacteria to nanostructured titanium surfaces: a systematic study. *Int. J. Nanomed.* **2017**, *12*, 1415–1430. [\[CrossRef\]](#)
98. Zhang, Y.; Bose, T.; Unger, R.E.; Jansen, J.A.; Kirkpatrick, C.J.; van den Beucken, J.J.J.P. Macrophage type modulates osteogenic differentiation of adipose tissue MSCs. *Cell Tissue. Res.* **2017**, *369*, 273–286. [\[CrossRef\]](#)
99. Linares, J.; Fernandez, A.B.; Feito, M.J.; Matesanz, M.C.; Sanchez-Salcedo, S.; Arcos, D.; Vallet-Regi, M.; Rojo, J.M.; Portoles, M.T. Effects of nanocrystalline hydroxyapatites on macrophage polarization. *J. Mater. Chem. B* **2016**, *4*, 1951–1959. [\[CrossRef\]](#)
100. Alhamdi, J.R.; Peng, T.; Al-Naggar, I.M.; Hawley, K.L.; Spiller, K.L.; Kuhn, L.T. Controlled M1-to-M2 transition of aged macrophages by calcium phosphate coatings. *Biomaterials* **2019**, *196*, 90–99. [\[CrossRef\]](#)
101. Li, X.; Huang, Q.; Elkhoory, T.A.; Liu, Y.; Wu, H.; Feng, Q.; Liu, L.; Fang, Y.; Zhu, W.; Hu, T. Effects of titanium surface roughness on the mediation of osteogenesis via modulating the immune response of macrophages. *Biomed. Mater.* **2018**, *13*, 045013. [\[CrossRef\]](#)

